Supplementary Figures

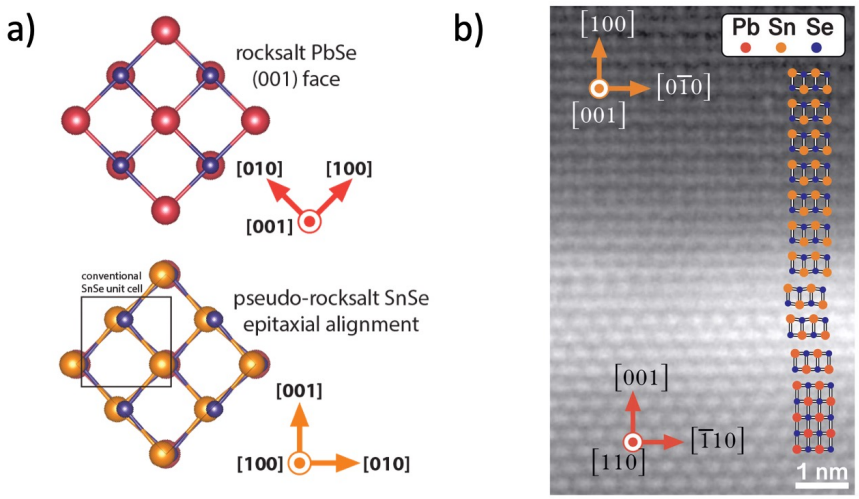

Figure S1: (a) The pseudo-rocksalt stacking of SnSe on PbSe, showing the similarity of the PbSe (001) surface and the SnSe (100) surface. The SnSe unit cell shown has been slightly strained to appear square. Note that even in this symmetrized form, SnSe has lower rotational symmetry than PbSe. (b) HAADF STEM showing the interface between an SnSe film and the PbSe interlayer.

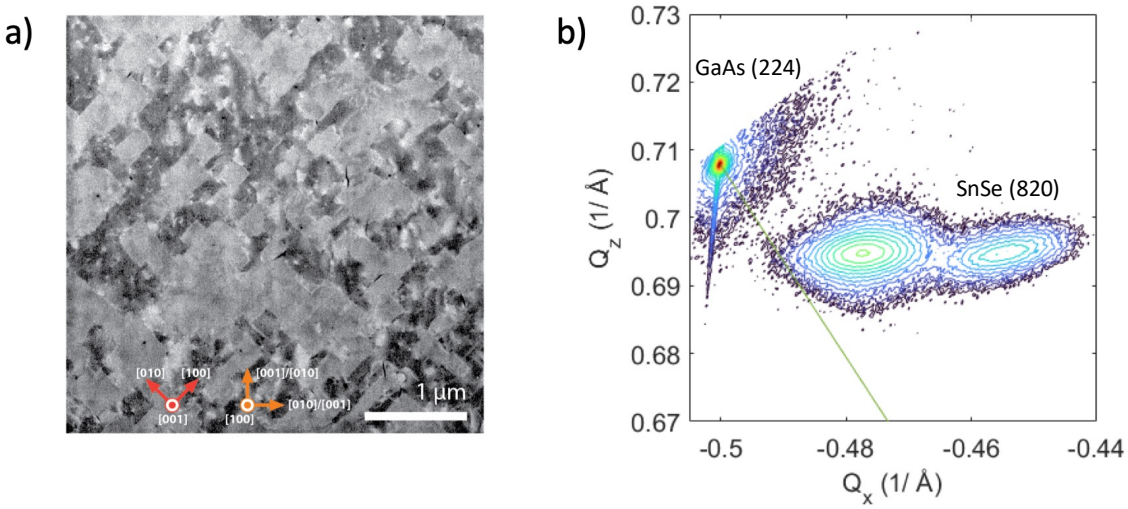

Figure S2: (a)Electron Channeling Contrast Imaging of a SnSe layer polished by FIB showing two populations of 90° rotated grains with rectangular grain boundaries, and threading dislocation contrast within one of those populations of grains. (b) Reciprocal space map of SnSe on GaAs, showing the GaAs (224) peak, and 2 peaks corresponding to the SnSe (820) diffraction condition, marking the two populations of 90° rotated SnSe grains.

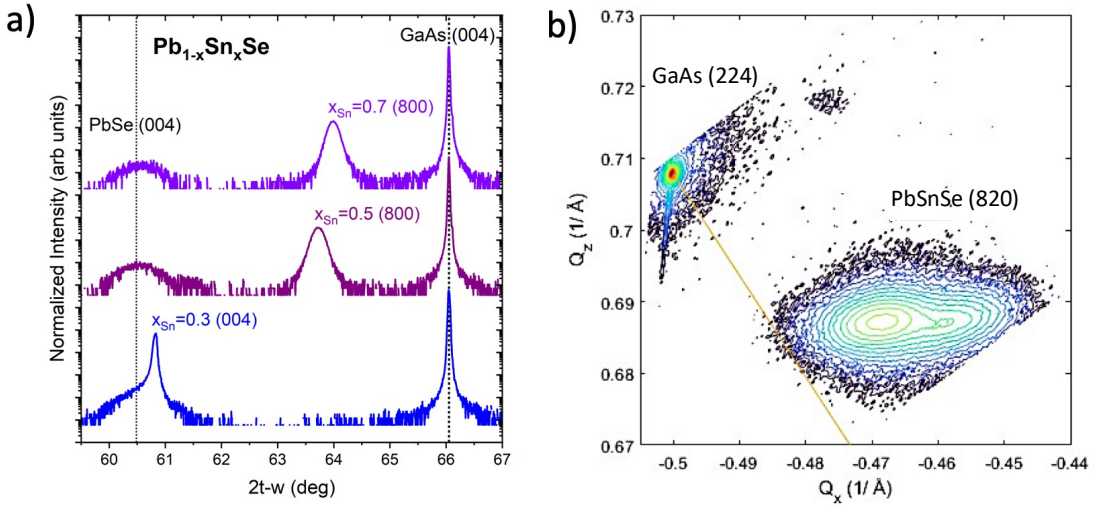

Figure S3: (a) Triple-axis 2θ-ω scan of various compositions of $Pb_{1-x}Sn_xSe$ alloys, including the GaAs (004) reflection. Also visible are the (800) and (004) peaks of PbSnSe, for the orthorhombic and cubic phase respectively. The alloy is cubic for the x=0.3 sample, and orthorhombic for the x=0.5 and 0.7 samples. (b)Reciprocal space map of $Pb_{0.5}Sn_{0.5}Se$ on GaAs, showing the GaAs (224) peak and (820) alloy peaks expected for a film in the orthorhombic phase.